Catalysis Science & Technology

PAPER

View Article Online
View Journal | View Issue

Cite this: *Catal. Sci. Technol.*, 2019, 9, 1669

Tin modified Nb_2O_5 as an efficient solid acid catalyst for the catalytic conversion of triose sugars to lactic acid†

Xincheng Wang, *[ab] Yongji Song,[ab] Long Huang,[ab] Hong Wang,[ab] Chongpin Huang[c] and Cuiqing Li[ab]

Lactic acid (LA) is a versatile platform chemical for the production of biodegradable plastics and starting materials for the chemical and pharmaceutical industries. In this study, bimetallic oxide catalysts based on niobia were prepared by a facile sol–gel method and used as heterogeneous solid acid catalysts for the conversion of triose sugars to LA under aqueous conditions. The coprecipitation of $KNbO_3$ and metal salts ensured the uniform dispersion of all the metal atoms and prevented the agglomeration of individual metal oxides. A phase transfer of the niobium species from corner-sharing to edge-sharing octahedra was observed after the incorporation of tetragonal tin species, endowing niobium oxides with promising catalytic activity. Pyridine Fourier transform infrared spectroscopy analysis demonstrated the presence of both Lewis and Brønsted acid sites, which played essential roles in the conversion of biomass sugars. The Brønsted-to-Lewis site ratio could be tuned by varying the amounts of the metal oxides. SnO_2-Incorporated niobia outperformed all the catalysts investigated, catalyzing the complete conversion of dihydroxyacetone at 160 °C to give a promising optimal LA yield of 98%. The product distribution depended closely on the reaction temperature, catalyst loading and substrate concentration. The metal–metal interactions between Sn and Nb could be observed by X-ray photoelectron spectroscopy, Raman spectroscopy, and UV-vis spectroscopy. In addition, a possible reaction mechanism was proposed; the anchoring of water molecules at the oxygen vacancies created by incorporating tin oxide into niobia greatly facilitated proton diffusion during the acid-catalyzed conversion of pyruvaldehyde to LA, which was found to be the rate-determining step. This method enables facile catalyst separation and recycling and provides an efficient strategy for the development of novel solid acid catalysts for converting carbohydrates to platform chemicals.

Received 3rd February 2019,
Accepted 1st March 2019

DOI: 10.1039/c9cy00257j

rsc.li/catalysis

Introduction

Biomass resources are abundant and can be a suitable renewable feedstock for producing fuels and platform chemicals to replace products obtained from fossil fuels.[1,2] Conventional liquid acids have long been used as catalysts for the transformation of carbohydrates.[3–5] However, the use of homogeneous liquid acids involves harsh reaction conditions and tedious distillation, neutralization, and separation procedures. Therefore, easily separable and reusable solid acid catalysts have become increasingly important for realizing a sustainable society. Zeolites are effective solid acid catalysts for the conversion of carbohydrates to platform chemicals such as lactic acid (LA), levulinic acid, and furfurals.[6] However, the preferred solvent is environmentally benign water, which would be very detrimental to zeolites, leading to the leaching of sites, loss of surface area or collapse of the pore architecture.[7] Niobic acid ($Nb_2O_5{\cdot}nH_2O$) has been used as a water-tolerant solid acid catalyst for various reactions, such as esterification, hydrolysis, and hydration.[8] Niobium oxide can be effectively supported on several oxidic materials, such as alumina, titania, and silica, which modulates their acidity and results in very active catalysts for dehydration reactions (for instance, dehydration of methanol to diethyl ether, dehydration of butanol, and dehydration of glycerol to acrolein).[9–11] It should be noted that the unique catalytic action of $Nb_2O_5{\cdot}nH_2O$ is attributed to its strong Brønsted acidity; however, the conversion of carbohydrates requires not only Brønsted acid sites but also Lewis acid sites.

[a] *Beijing Key Laboratory of Fuels Cleaning and Advanced Catalytic Emission Reduction Technology, Beijing 102617, China. E-mail: wxcnathan@gmail.com, wangxc@bipt.edu.cn*
[b] *College of Chemical Engineering, Beijing Institute of Petrochemical Technology, Beijing 102617, China*
[c] *State Key Laboratory of Chemical Resource Engineering, Beijing University of Chemical Technology, Beijing 100029, China*

† Electronic supplementary information (ESI) available: NH_3-TPD profiles of SnO_2/Nb_2O_5 and characterization of recycled SnO_2/Nb_2O_5-3.07. See DOI: 10.1039/c9cy00257j

Tin-modified beta zeolites (Sn-BEA) were reported to contain Lewis acid sites that selectively catalyze the isomerization of glucose to fructose under aqueous conditions.[12,13] Promising yields of LA were achieved from the conversion of dihydroxyacetone (DHA) in water after 24 h at 125 °C using a Sn-beta zeolite[14] (90 mol%) and an ultrastable Y zeolite (H-USY)[15] (71 mol%). A relatively high selectivity to LA (83%) at 92% DHA conversion was achieved at 110 °C after 6 h over a Sn–Si-CSM catalyst.[16] Dapsens *et al.*[17] reported that an LA selectivity higher than 90% (up to 92%) could be obtained with desilicated ZSM-5 in solutions of alkali metal hydroxides. The same group has demonstrated tin-containing MFI zeolites as selective and recyclable catalysts able to operate in both aqueous and methanolic solutions of DHA.[18] In addition, Cr, Al, Zr, and Ti have been demonstrated to be catalytically active components of zeolites during the conversion of DHA to methyl lactate. Methyl lactate formation from triose sugars in methanol is an excellent example of utilizing the Lewis acidity of metal-modified zeolites for selective biomass conversion.[14] However, zeolite catalysts suffer from deactivation during LA formation in water due to the leaching of the active metal species in the acidic reaction mixture or to the collapse of the pore architecture.[19]

Niobium oxides were shown to have both Brønsted and Lewis acid sites, and their quantities and strengths could be tuned.[20] Coordinately unsaturated Nb sites on a deformed orthorhombic niobium oxide phase were recently reported to act as water-tolerant Lewis acid sites in the formation of LA from a triose sugar in water.[8] The presence of Nb–OH groups provides Brønsted acidity, whereas coordinatively unsaturated Nb^{5+} sites impart Lewis acidity, as revealed by acetonitrile adsorption followed by FTIR spectroscopy.[9] The combination of Brønsted and Lewis acidity is potentially useful for the formation of lactic acid from triose sugars because the surface acidity can be tuned for the dehydration and isomerization reactions of DHA. Different combinations of active sites (metals), supports and promoters have been reviewed by Dumesic *et al.* for effective catalyst optimization. The use of bimetallic catalysts is a promising option for upgrading biomass feedstocks to make liquid fuels.[21] A combination of homogeneous indium chloride and tin chloride was reported to synergistically catalyze the formation of methyl lactate from sugars with a maximum yield of 72%.[22] A combination of Al(III) and Sn(II) cations was also found to be efficient for catalyzing the conversion of cellulose and related carbohydrates to LA.[23] This report motivated our study of dual metal oxide acid catalysts based on niobium oxide for the selective production of LA from DHA, which can be obtained by the fermentation or stoichiometric or catalytic oxidation of glycerol. Indeed, DHA is commonly used to study the effects of various catalysts because its fundamental carbon structure is similar to that of LA.[24]

Mesoporous Nb_2O_5–MeO_2 (Me═Ti, Zr, Ce) mixed oxides were previously prepared by an evaporation-induced self-assembly method and used in the dehydration of fructose to 5-hydroxymethylfurfural and levulinic acid.[25,26] In this study, metal oxide-modified Nb_2O_5 solid acid catalysts with both Lewis and Brønsted acid sites were synthesized by a simple coprecipitation method in water at 160 °C for three days. The effects of different metal sites on Nb_2O_5 were carefully explored by performing a triose sugar conversion reaction in the green solvent water.[27] The Lewis and Brønsted acidity of tin-modified Nb_2O_5 in the presence and absence of physisorbed water was studied by pyridine FTIR spectroscopy. In addition, the interactions between tin and niobium were investigated by Raman spectroscopy, UV-vis, and XPS analysis. The yields were optimized by varying the process conditions, including the reaction temperature, catalyst loading and substrate concentration. A plausible reaction mechanism describing the role of water molecules was then proposed.

Results and discussion

X-ray diffraction and TEM analysis

The coprecipitation of alkaline $KNbO_3$ and acidic $SnCl_4$ solutions ensured the uniform dispersion of the Sn and Nb atoms, which led to uniform metal oxides and prevented the agglomeration of individual metal oxides. The TEM images show that the Sn-doped niobium oxides were composed of nano particles with small void spaces, which contributed to the surface area and pore volume. As shown in Fig. 1a, the SnO_2/Nb_2O_5 particles were relatively homogeneous in size and shape with a size of approximately 5 nm. Fig. 1b shows the HRTEM image of SnO_2/Nb_2O_5. The clear lattice fringes indicated good crystallinity, and the lattice spacing of 0.28 nm corresponded to the (101) planes of tetragonal SnO_2. The crystal structure of these samples was tetragonal SnO_2, as confirmed by the appearance of the (110), (101), (200), (211), (220) and (301) diffraction peaks according to JCPDS No. 41-1445 as shown in Fig. 2a. Furthermore, the as-synthesized Nb_2O_5 catalysts generally had higher specific surface areas than the commercial samples (Table 1, entry 2 *vs.* entry 8). After the incorporation of tin, the surface area was 220 $m^2\ g^{-1}$, which is comparable to that of *ortho*-Nb_2O_5.[8]

The SAED pattern in Fig. 1 indicates that the Sn-doped Nb_2O_5 was polycrystalline.[30] Nb^{5+} doping might induce a distortion of the lattice constants of the SnO_2 unit cell because Nb has a larger ionic radius than Sn. This structural distortion was observed by HRTEM. In particular, the image of the

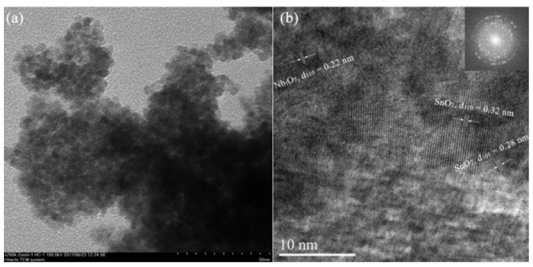

Fig. 1 (a) TEM and (b) high-resolution TEM (HRTEM) images of SnO_2/Nb_2O_5-3.07.

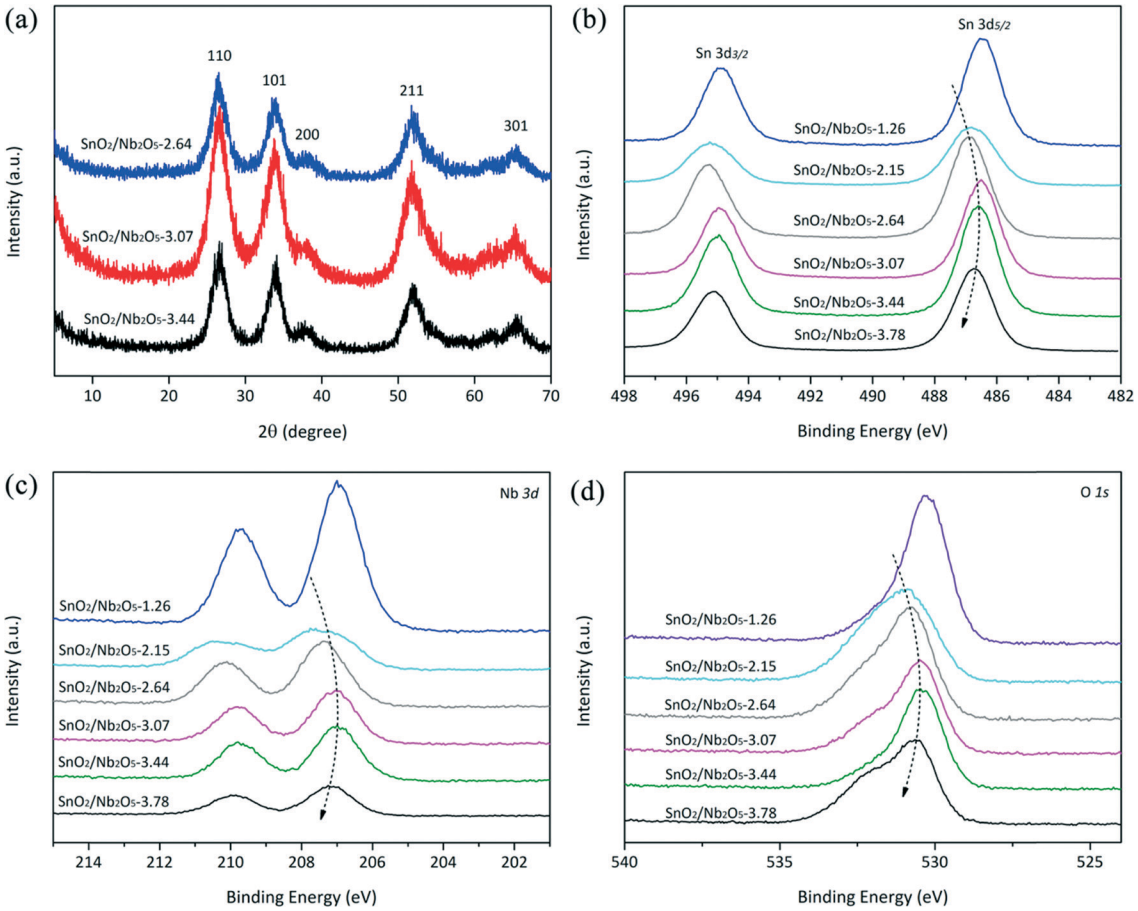

Fig. 2 X-ray diffraction patterns (a) and XPS spectra (b–d) of the SnO_2/Nb_2O_5 samples.

Table 1 Catalytic conversion of DHA to LA by Nb_2O_5-based catalysts ($[DHA]_o$ = 0.2 M; catalyst (metal/Nb = 3.0) = 50 mg; 140 °C; 1 h)

Entry	Catalyst	Specific surface area ($m^2\ g^{-1}$)	Total acid sites[b] (mmol g^{-1})	BAS/LAS ratio[c]	GLA (%)	PA (%)	LA (%)	DHA conv. (%)
1	SnO_2	109.3	0.12	0.15	0.2	4.2	5.8	17.6
2	Nb_2O_5[a]	195	0.37	0.81	0.5	48.1	30.2	94.5
3	SnO_2/Nb_2O_5	220	0.56	0.36	0.6	3.1	86.3	99.9
4	Al_2O_3/Nb_2O_5	185	0.31	0.67	1.3	23.5	49.3	95.4
5	PbO/Nb_2O_5	93	0.25	0.79	0.75	31.4	20.3	93.9
6	CdO/Nb_2O_5	97	0.22	0.83	0.83	35.6	18.3	91.5
7	Cr_2O_3/Nb_2O_5	165	0.50	0.41	1.6	1.2	71.4	98.5
8	Nb_2O_5-C[d]	155	0.16	4.88	1.9	31.6	2.8	40.9
9	SnO_2/Nb_2O_5-C	141	0.23	1.62	2.1	56.6	17.4	76.4
10	Cr_2O_3/Nb_2O_5-C	138	0.19	1.83	1.2	43.5	13.5	58.2
11	CdO/Nb_2O_5-C	85	0.11	4.65	1.0	35.5	12.9	57.6
12	PbO/Nb_2O_5-C	76	0.09	4.91	1.5	30.0	12.1	56.3
13	Al_2O_3/Nb_2O_5-C	119	0.15	5.32	1.1	44.2	13.1	63.1

[a] Potassium niobate was precipitated by adding acetic acid. [b] Determined by NH_3-TPD analysis. [c] The Brønsted/Lewis site (BAS/LAS) ratio was determined by monitoring the pyridine desorption at 150 °C with FTIR. [d] Nb_2O_5-C refers to commercial Nb_2O_5. Note: the abbreviations do not suggest any stoichiometric composition.

lattice fringe in Fig. 1b shows an interplanar distance of d110 = 0.32 nm, whereas d110 = 0.34 nm for pure-phase SnO_2. In contrast, due to the tin cation doping of the nanospheres and related lattice expansion, the d110 value of Nb_2O_5 was measured to be 0.22 nm, compared to the value of 0.18 nm for pure-phase Nb_2O_5 (JCPDS No. 28-0317).

XPS analysis

The surface compositions and elemental states of the SnO_2/Nb_2O_5 samples were investigated by XPS. As shown in Fig. 2b, the $3d_{5/2}$ and $3d_{3/2}$ spin orbital peaks of SnO_2 could be fitted by doublets with binding energies of 486.29 eV and

494.73 eV, respectively, which is characteristic of tetravalent tin.[28] The Nb 3d XPS spectra exhibit a single symmetric $3d_{5/2}$ component with a BE value of approximately 207 eV, which was assigned to Nb^{5+}; no evidence of the presence of Nb^{4+} was observed.[26] Because SnO_2 has a higher electronegativity, it was expected to withdraw electrons from Nb_2O_5, and its binding energy was expected to shift to lower values with increasing amount of SnO_2. However, this effect was reversible; the BE values of Sn^{4+} shifted to higher energies for SnO_2/Nb_2O_5-3.78. Interestingly, the peaks of Nb followed the same trend. This shift could be attributed to the change in their coordination numbers; in other words, the oxygen vacancies were also proposed to contribute to the shifting trend of Sn and Nb. Moreover, it could indicate interactions between the Sn and Nb atoms in the oxides.[26] The binding energy shift could also be due to the presence of lattice strain, which was observed in the HRTEM analysis.[31] It should be noted that the interactions between Sn and Nb should be further verified by extended X-ray absorption fine structure experiments.

The O 1s peak was broad and complex, as shown in Fig. 2d. The peak shape suggested the existence of multiple peaks representing the overlapping contributions of oxygen in different chemical states.[26] The peak at approximately 530 eV was attributed to the lattice oxygen in both tin and niobium oxides. The shoulder at 532.5 eV could be attributed to chemisorbed oxygen and the oxygen in hydroxyl groups. The surface Sn/Nb ratios were obtained from the quantitative XPS results (Table S1†). The difference between the surface and bulk ratios clearly shows the relative enrichment in Sn at the surfaces of the mixed oxides. Because the Lewis acidity is mainly derived from the surface Sn species, this enrichment is beneficial for Lewis acid-catalyzed cascade reactions. Similar binding energy shifting trends for Sn 3d, Nb 3d, and O 1s indicated the distortion in the crystal lattice, which was supposed to imitate the austenitic lattice expansion–contraction–expansion, leading to the superior catalytic activity of SnO_2/Nb_2O_5-3.07.

Raman spectroscopy

To determine the oxidation state and surface characteristics, Raman vibrational spectra of the tin-niobium oxides were collected (Fig. 3a). The vibrational band in the range of 800–900 cm^{-1} was attributed to the symmetric stretching mode of Nb═O species in highly distorted NbO_6 octahedra.[32] The peak at approximately 450 cm^{-1} corresponded to the E_g mode of SnO_2, whereas the well-defined peak at approximately 632 cm^{-1} was assigned to the A_{1g} symmetric Sn–O stretching mode of SnO_2.[33] The E_g mode is the most sensitive to oxygen vacancies, and its occurrence in niobium oxides with higher tin oxide amounts indicated the presence of vacancies.[34] All the samples exhibited a mode at approximately 256 cm^{-1}, possibly due to the formation of SnO_2 nanoparticles, which is supported by the TEM results. Meanwhile, the intense band centered at 160 cm^{-1} indicated the presence of a substoichiometric SnO_x ($1 < x < 2$) intermediate between SnO and SnO_2,[31] suggesting the existence of oxygen vacancies.

UV-vis absorption

UV-vis DRS on calcined samples was used to investigate the electronic properties of tin and niobium species (Fig. 3b). No bulk SnO_2 species was present in the calcined SnO_2/Nb_2O_5 catalysts because of the absence of UV-vis bands near 300 nm. Indeed, the incorporation of tin affected the coordination structure of niobium with the disappearance of absorption band of corner-sharing NbO_6 octahedra at ~320 nm, resulting in lowered coordination symmetry of Nb atoms.[35] The UV-vis DRS spectra show broad bands ranging from 220 to 250 nm, suggesting the overlap of oligomeric tetrahedral Sn oxide species and edge-sharing octahedral niobium species.[36] Therefore, the structure of niobium species transformed from corner-sharing to edge-sharing octahedra when tetragonal tin species was incorporated. The absorption maximum of the hybrid catalysts showed no shift and the intensity increased along with the increase of tin loading, indicating the constant size of the metal oxide particles.

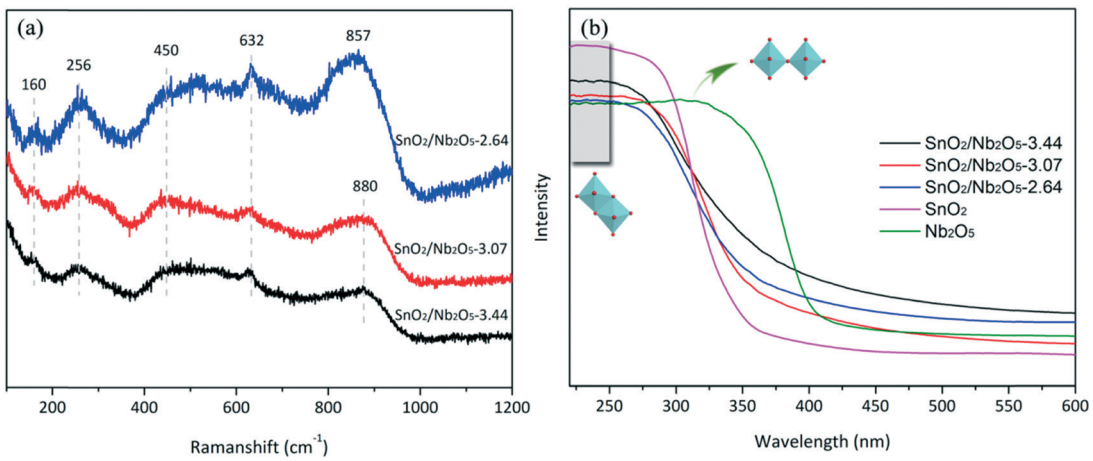

Fig. 3 Raman (a) and UV-vis DRS (b) spectra of SnO_2/Nb_2O_5.

Acidity evaluation by NH_3-TPD and FTIR spectroscopy of adsorbed pyridine

The acidic properties of SnO_2/Nb_2O_5 were determined by NH_3 temperature-programmed desorption (TPD). The low-temperature desorption of NH_3 indicated the presence of weak acid sites, and the NH_3 desorption profiles are shown in Fig. S2.† Increasing the tin content had a negative effect on the total acid density, and the total acid sites continuously decreased from 0.65 mmol g^{-1} to 0.30 mmol g^{-1} when the Sn/Nb ratio increased from 1.26 to 3.78. Compared to the as-synthesized Nb_2O_5 sample, the amount of weak acid sites in the Sn–Nb binary oxide sample (after Sn doping) was clearly higher. Moreover, it was proposed that medium acid sites formed during calcination because only a small amount of medium acid sites was observed in the profile of raw SnO_2/Nb_2O_5-3.78. The use of Al, Pb, and Cd greatly decreased the amount of total acid sites, but this decrease was not observed for the Cr-doped materials (Table 1, entries 4–7).

The acidic properties of SnO_2/Nb_2O_5 were also studied by monitoring pyridine adsorption by *in situ* IR spectroscopy to evaluate the surface Lewis/Brønsted character (Fig. 4). The bands at 1450, 1489 and 1540 cm^{-1} were attributed to the Lewis acid sites, overlap of the Brønsted and Lewis acid sites, and Brønsted acid sites, respectively.[37] The IR analysis showed that the intensities decreased as the desorption temperature was increased from 100 to 400 °C. The relative Brønsted-to-Lewis acidity ratios (BAS/LAS ratios) could be deduced by integrating the areas under the characteristic bands while taking into account the extinction coefficients.[15] The BAS/LAS ratio increased with decreasing Sn amount (0.73, 0.55, 0.44, 0.36, 0.31, and 0.23 for Sn/Nb ratios of 1.26, 2.15, 2.64, 3.07, 3.44, and 3.78, respectively). This result is consistent with the fact that niobium oxides are stronger solid acid catalysts than tin oxides, especially in terms of the Brønsted acidity. However, strong Brønsted acidity is unfavorable for obtaining high LA yields from triose sugars. The *in situ* incorporation of SnO_2 into Nb_2O_5 was shown to increase the highly favorable Lewis acidity. The Lewis acidity of SnO_2/Nb_2O_5 was strong enough to be maintained after outgassing at 400 °C for 1 h (Fig. 4a), but the Brønsted acidity could only be observed at 150 °C. In addition, the total acid sites of the as-synthesized materials were generally higher than those of the commercial Nb_2O_5-based catalysts, whereas the opposite trend was observed for the BAS/LAS ratio.

The characterization of the nature of the surface acid sites is very important for optimizing the reaction parameters and understanding the reaction and deactivation mechanisms. To determine the water tolerance of the sample, SnO_2/Nb_2O_5 was first calcined at 500 °C and then exposed to water vapor at 150 °C. Then, the sample was outgassed at room temperature for 1 h and subjected to a pyridine adsorption–desorption procedure. Both Brønsted and Lewis acid sites were detected, indicating that some of the Lewis acid sites on SnO_2/Nb_2O_5 acted as water-tolerant active sites (Fig. 4b). Moreover, the formation of Brønsted acid sites was also observed after the water vapor treatment. Thus, water-induced Lewis and Brønsted acid sites were expected to be the active sites. The catalytic mechanism is discussed below.

Catalyst screening

When methanol was used as the solvent, no methyl lactate was obtained under the same reaction conditions, indicating that water performed essential functions during the conversion of DHA to LA. Indeed, DHA first underwent a dehydration reaction to PA, as revealed by an investigation of the reaction profiles (Fig. 5a). Then, PA was further rehydrated and converted to LA *via* a 1,2-hydride shift. DHA was completely converted after 2 h with only a trace amount of glyceraldehyde remaining, whereas PA reached an optimal yield of 63% after 40 min. On the other hand, water was expected to affect the surface acidity of the catalysts by adjusting the relative amounts of the Lewis and Brønsted sites. Therefore, investigating the surface acidity under vacuum conditions does not accurately capture the *in situ* surface acidity. In this study, the evolution of the Lewis/Brønsted ratio was investigated by

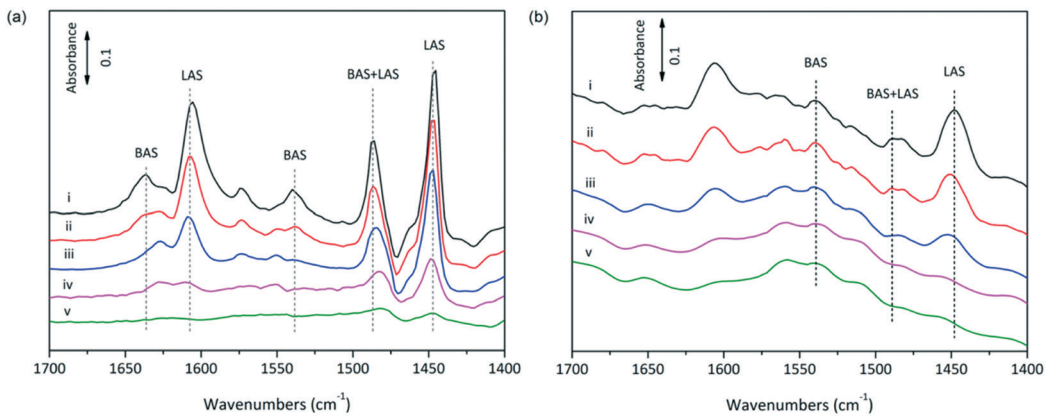

Fig. 4 (a) SnO_2/Nb_2O_5-3.07 and (b) SnO_2/Nb_2O_5-3.07 treated at 500 °C for 1 h, then exposed to water vapor at 150 °C for another 1 h, outgassed at room temperature and subjected to a pyridine adsorption–desorption procedure.

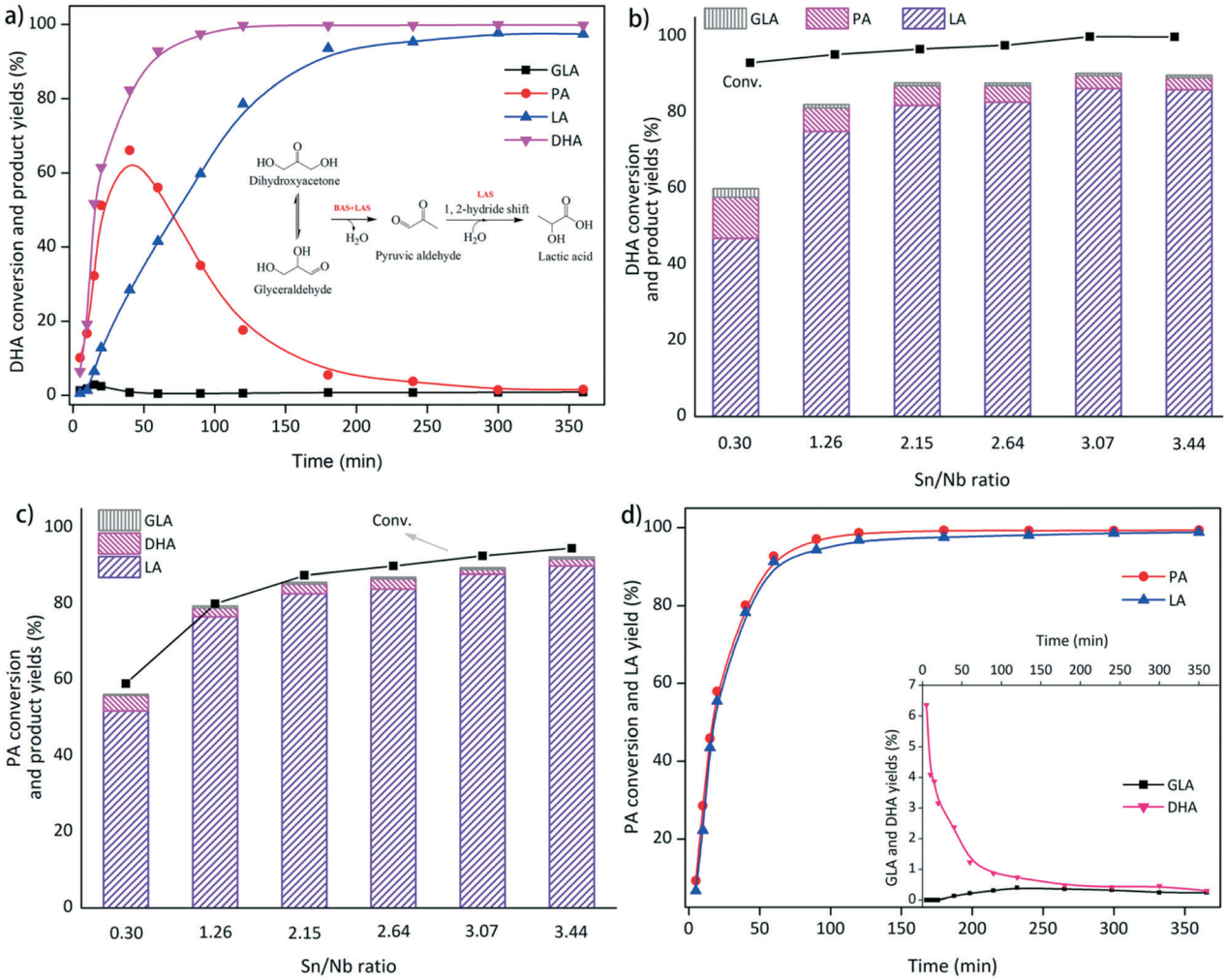

Fig. 5 a) Time evolution of the DHA conversion over SnO_2/Nb_2O_5-3.07 ($[DHA]_o$ = 0.2 M, catalyst = 50 mg, T = 120 °C. Inset: Reaction pathway). b) Conversion of DHA over SnO_2/Nb_2O_5 with different surface Sn/Nb ratios (the Sn/Nb ratios were determined by XPS analysis) ($[DHA]_o$ = 0.2 M, catalyst = 50 mg, T = 140 °C, time = 1 h). c) Conversion of PA over SnO_2/Nb_2O_5 with different surface Sn/Nb ratios (the Sn/Nb ratios were determined by XPS analysis) ($[PA]_o$ = 0.2 M, catalyst = 50 mg, T = 140 °C, time = 1 h). d) Time evolution of the PA conversion over the SnO_2/Nb_2O_5 catalysts ($[PA]_o$ = 0.05 M, catalyst (Sn/Nb ratio = 3.07) = 50 mg, T = 140 °C).

introducing water molecules during the characterization of the acidity as previously described.

To investigate the catalytic performance of SnO_2/Nb_2O_5 with different metal salts, the LA yields of the reaction of DHA in water at 140 °C were measured (the results are listed in Table 1, entries 1–7). Only a small amount of LA was obtained for the blank reaction without a catalyst, although the PA yield was 22.6%. The metal-to-niobium ratios were kept constant as 3.0. Nearly complete DHA conversion was achieved with all the readily synthesized metal-modified niobium oxides except for pure SnO_2. Pure Nb_2O_5 gave a promising PA yield of 48.1% and LA yield of 30.2%, while pure SnO_2 gave a PA yield of 4.2% and LA yield of 5.8%. Obviously, the tin-modified Nb_2O_5 outperformed all of the prepared materials with LA and PA yields of 86.3% and 3.1%, respectively. Comparable LA yields were achieved with Cr_2O_3/Nb_2O_5 and SnO_2/Nb_2O_5; however, a much lower PA yield was obtained with Cr_2O_3/Nb_2O_5, indicating that the dehydration of DHA to PA might not be the rate-determining step of the cascade reaction.[38] When Al was used, the dominant product was LA with a yield of 49.3%, which is comparable to the yield of methyl lactate obtained by the steamed Al-beta-catalyzed reaction of DHA in methanol.[14] Of course, water is a more environmentally benign solvent than methanol, and the preparation method of the mixed metal oxides in this work is simpler than that of steamed beta zeolites. Using the Pb- and Cd-modified Nb_2O_5 resulted in LA yields of 20.3% and 18.3%, respectively, and moderate PA yields.

Commercial Nb_2O_5 was used to demonstrate the effects of both the metal salts and the supports (Table 1, entries 8–13). Clearly, commercial Nb_2O_5 could catalyze the dehydration of DHA to PA; yields of over 30% were obtained with all the samples. The highest PA yield of 56.6% was achieved with the Sn-doped oxide. The conversions of DHA varied from 40.9% to 76.4%, and the yields of LA were approximately 13%, except in the case of SnO_2/Nb_2O_5-C (17.4%). Therefore,

the use of tin salts not only promoted the dehydration reaction of DHA but also enhanced the subsequent reactions leading to the formation of LA.

The effects of the surface tin-to-niobium ratios were investigated in the range of 0.30 to 3.44 at 140 °C to optimize the material (Fig. 5b). The conversion of DHA increased gradually from 93% to 99%. A sudden improvement in the LA yield from 47% to 75% was observed when the surface Sn/Nb ratio increased from 0.3 to 1.26. Above this ratio, the yield of LA increased slightly to 86% at an Sn/Nb ratio of 3.07, and the

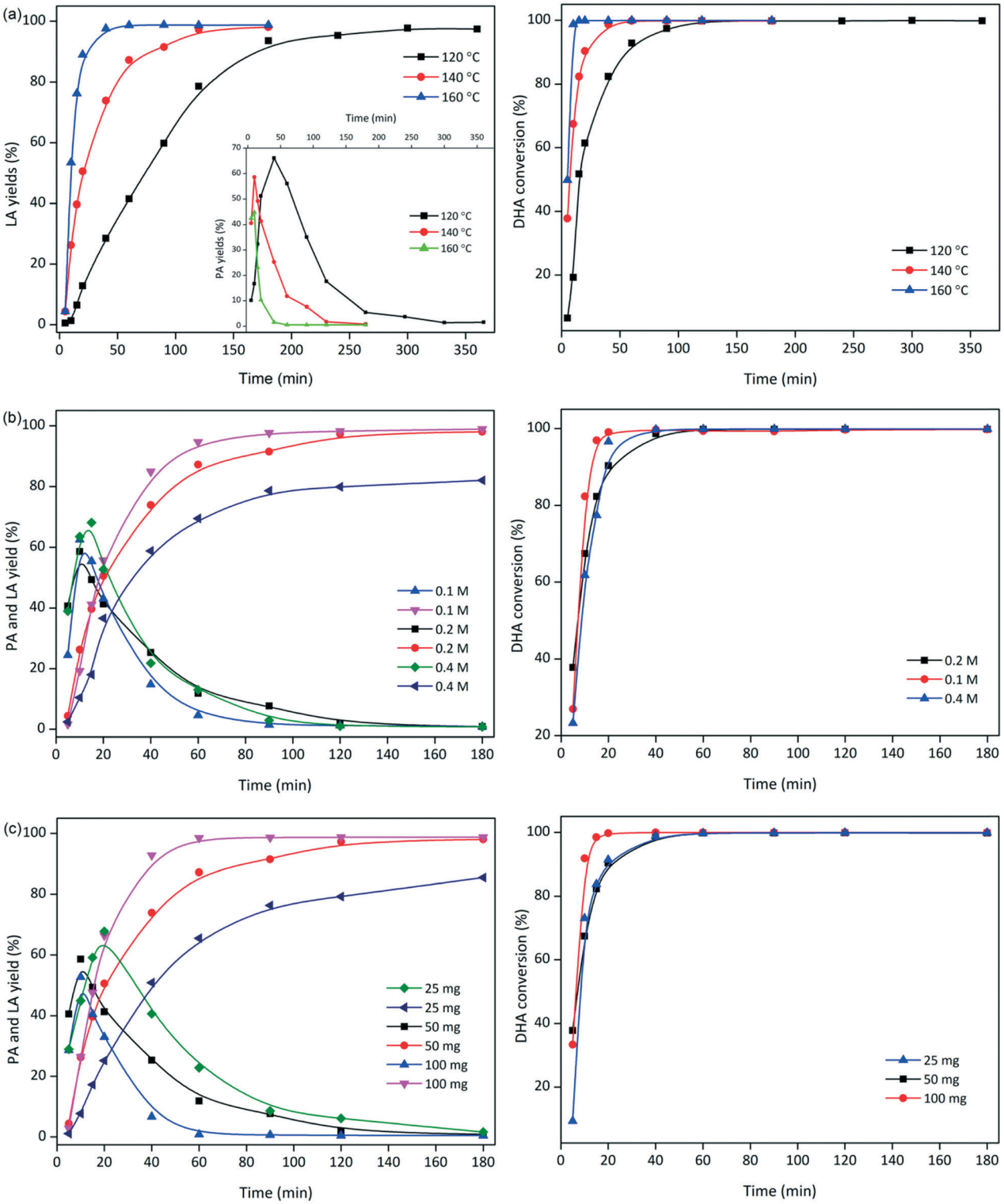

Fig. 6 Optimization of the reaction conditions: (a) reaction temperature, (b) substrate concentration, and (c) catalyst loading (conditions: $[DHA]_o$ = 0.2 M, SnO_2/Nb_2O_5-3.07 = 50 mg, 140 °C).

formation of PA gradually decreased from 6.2% to 3.1%. The yield of LA remained constant at a higher Sn/Nb ratio of 3.44. Thus, the promoting effect of Sn on the transformation of DHA to LA was further confirmed.

PA was determined to be the intermediate in this reaction system. Therefore, PA was used as a reactant to further explore the efficiency of the SnO_2/Nb_2O_5 samples for the production of LA (Fig. 5c). The yield of LA increased gradually with the conversion of PA, and a final LA yield of *ca.* 90% was obtained over SnO_2/Nb_2O_5-3.44 at 140 °C after 1 h. The LA selectivity from PA was clearly higher than that from DHA over the same sample. Generally, hydrated PA was assumed to be a key intermediate for the production of LA from PA. However, the formation of GLA and DHA were observed, indicating the reversibility of the dehydration–rehydration reactions between GLA or DHA and PA (Fig. 5c and d). An LA selectivity as high as 97% was obtained from PA conversion over $Sn_{3.07}/Nb_2O_5$ after 90 min, as shown in Fig. 5d. The yield of LA increased with the conversion of PA, and a final LA yield of 98% was obtained at 140 °C after 2 h. Therefore, a Sn/Nb ratio of 3.07 was selected for more in-depth studies.

Optimization of the process conditions for the conversion of DHA to LA catalyzed by SnO_2/Nb_2O_5-3.07

To gain insight into the effects of the process conditions during the transformation of DHA to LA, the liquid products obtained using SnO_2/Nb_2O_5-3.07 were identified and quantified by HPLC analysis. The conversion of DHA and yields of PA and LA depended strongly on the reaction temperature (Fig. 6a). The conversion rate increased dramatically with increasing temperature, and an essentially quantitative conversion of DHA (99%) was achieved within 15 min at 160 °C. At 120 °C, a reaction time of 120 min was required to reach *ca.* 99% conversion. The yield of LA increased significantly with an increase in the temperature from 120 °C to 160 °C; a maximum LA yield of 98.7% was obtained at 160 °C. However, low temperatures tended to favor the formation of PA; the highest yield of 66% was achieved at 120 °C. In addition, the color of the reaction solution changed from yellow to dark brown with increasing temperature, indicating the formation of humins.[39]

The effects of the initial DHA concentration on the DHA conversion and product yields are presented in Fig. 6b. High yields of LA were expected at low initial substrate concentrations. More PA was formed at high initial DHA loadings, but the time required to reach the optimal PA yield was generally the same. The formation of brown soluble materials was also observed at high concentrations of DHA.[40] The effects of the SnO_2/Nb_2O_5-3.07 dosage on the conversion of DHA and the yields of PA and LA are presented in Fig. 6c. Evidently, a high catalyst loading was beneficial for the conversion of DHA and the production of LA. In contrast, more PA was formed at low catalyst loadings, suggesting that SnO_2/Nb_2O_5-3.07 efficiently catalyzed the transformation of PA to LA under these reaction conditions. Furthermore, the effect of the initial PA concentration on the yield of LA is presented in Fig. 7. The PA conversion increased slightly in the range of 0.025 M to 0.2 M. However, the LA yield decreased dramatically to *ca.* 50% with increasing PA concentration, possibly due to the formation of humins at high substrate concentrations. Both GLA and DHA tended to decrease in the PA concentration range studied.

To verify the reusability of the catalyst, six consecutive reactions were conducted with SnO_2/Nb_2O_5-3.07 under the same reaction conditions after catalyst recovery (Fig. 8). Between runs, the catalyst was dried at 60 °C overnight and calcined at 500 °C. For each run, the catalyst was weighed to maintain a constant substrate-to-catalyst ratio. Complete conversion of DHA was observed without a significant loss of the LA yield after six consecutive runs, demonstrating that the catalyst was recyclable. The yield of PA increased slightly with the number of recycling runs. However, the formation of humins during the reactions was inevitable, and the deposited organic compounds could be substantially removed after calcination, preventing the detrimental effects of carbon deposition. The crystalline structure was maintained even after the sixth run (Fig. S3†). There is no significant change in the XPS, Raman, and UV-vis DRS spectra of the recycled catalysts

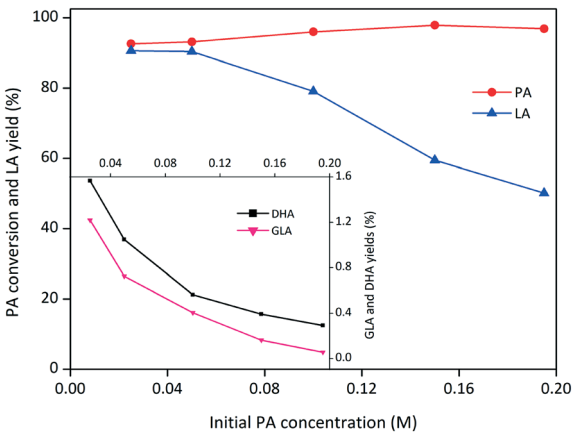

Fig. 7 Effect of the initial PA concentration on the conversion of PA to LA catalyzed by SnO_2/Nb_2O_5-3.07 (conditions: catalyst = 50 mg, 140 °C, 1 h).

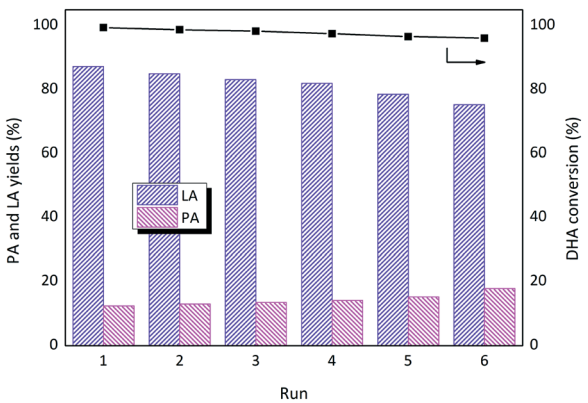

Fig. 8 Results of the reusability study (conditions: $[DHA]_o$ = 0.2 M, SnO_2/Nb_2O_5-3.07 = 50 mg, 140 °C, 1 h).

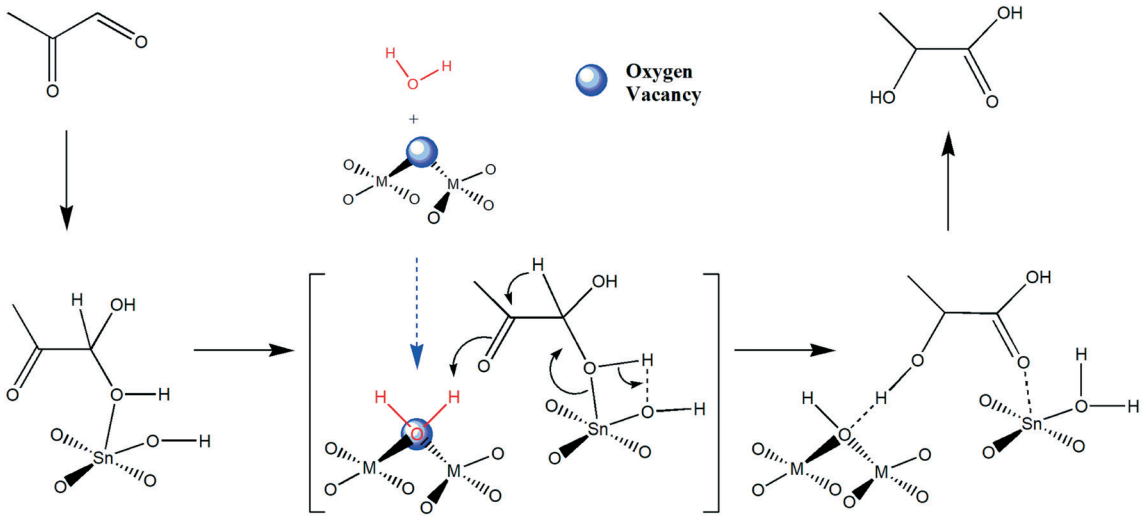

Scheme 1 Proposed reaction mechanism for the isomerization of hydrated PA to LA in this system (M: metal sites).

(Fig. S4†). Moreover, the SEM morphology of the recycled SnO_2/Nb_2O_5-3.07 was similar to that of the fresh sample (Fig. S1†). ICP analysis indicated that less than 2.3% of the initial metal content (both Sn and Nb) was lost, and the Sn/Nb ratio was slightly lower (2.6). However, the leaching of Sn from the surface was higher than that of Nb (surface Sn/Nb ratio: 3.1 *vs.* 2.6), suggesting that the Nb species were more stable than the Sn species under aqueous conditions. The loss of Sn resulted in an increase in the Brønsted/Lewis ratio, confirming that the Sn species were responsible for the Lewis acid sites (Table S1†). Only slight losses in the specific surface area and total acid sites were observed after six consecutive runs. Therefore, the prepared Sn–Nb mixed oxide catalysts exhibited good thermal stability and water tolerance and are promising solid acid catalysts for the conversion of carbohydrates to furan derivatives. Indeed, the products were dominated by 5-hydroxymethylfurfural or furfural (yields of 52%, 61%, and 33%, respectively), when glucose, fructose, and xylose were used as substrates under the same reaction conditions, suggesting the priority of dehydration reactions.

Mechanism investigation

The SnO_2/Nb_2O_5 catalysts efficiently facilitated the conversion of DHA to LA, which included the dehydration of DHA to PA, rehydration of PA and 1,2-hydride shift of hydrated PA to LA, due to their water-tolerant Lewis acid properties. Obviously, the dehydration of DHA was relatively fast due to the high acidity of SnO_2/Nb_2O_5, that is, the isomerization of PA to LA was the rate-determining step. It was reported that the isomerization of the intermediate PA to LA involves a Meerwein–Ponndorf–Verley reduction and Oppenauer oxidation (MPVO)-type redox step that is catalyzed only by Lewis acids.[40] Typically, a partially hydrolyzed framework tin species is believed to be the active site.[14] Herein, it was assumed that water would facilitate the proton transfer during the 1,2-hydride shift reaction (Scheme 1).[11] On the one hand, the oxygen vacancies were expected to act as anchoring sites for water molecules during the reaction, facilitating proton transfer. On the other hand, the metal sites adjacent to the oxygen vacancies tend to be more susceptible to partial hydrolysis and thus would have transformed into active sites for the isomerization reaction of PA. Lewis acid sites were also present on the surface in the form of coordinatively unsaturated Nb(v) sites. In this study, the niobium sites were responsible for the dehydration of DHA to PA, and the subsequent isomerization reaction of PA to LA occurred at the Nb and Sn sites. The strong interaction between these two sites makes the Sn/Nb_2O_5 catalysts suitable for the conversion of DHA to LA, and the reaction mechanism is depicted in Scheme 1. Proton diffusion on metal oxide surfaces can play an important role in many catalytic processes. It was assumed that the presence of water would accelerate proton diffusion during the 1,2-hydride shift reaction. Merte *et al.* investigated proton diffusion on an iron oxide thin film using high-speed, high-resolution scanning tunneling microscopy.[41] On oxygen-terminated FeO monolayer films formed on Pt, the presence of molecular water accelerated proton diffusion. Based on DFT calculations, these researchers proposed that a H_3O^+ transition state formed during the diffusion process. The effects of water molecules should be further investigated by hydrogen isotope reactions with water molecules to determine the hydrogen source of the hydroxyl group of LA.

Conclusions

This work presented a preliminary study of the use of metal oxide-modified niobia catalysts for the isomerization of triose sugars to LA. Tetravalent tin outperformed all the metals investigated, and the optimal Sn/Nb molar ratio was 3.07. The product distribution depended closely on the substrate concentration, reaction temperature, catalyst loading, and reaction time. An optimal LA yield of 98.7% was obtained at 160 °C after 4 h. Water-tolerant Lewis acid sites significantly

promoted the isomerization of PA, which was the rate-determining step during the conversion of DHA to LA. It was assumed that the strong interactions between Sn and Nb efficiently promoted the catalytic activity. A possible reaction mechanism for the isomerization of PA to LA was proposed. The excellent performance of the tin-modified niobia solid acid catalysts might motivate further study of the effects of metal–metal or metal–support interactions during the synthesis of solid acid catalysts for the conversion of carbohydrates.

Experimental

Sn/Nb_2O_5 was prepared by the simple coprecipitation of aqueous $SnCl_4$ with potassium niobate. The preparation of the potassium niobate solution was previously reported by the same author.[28] In a typical process, a certain amount of the $SnCl_4$ solution (0.3 M) was added dropwise to the potassium niobate solution (0.1 M) under vigorous stirring. The resulting white colloidal mixture was maintained at 160 °C for 3 days for crystallization. The white powder catalyst was then obtained by filtration, washed with deionized water, vacuum dried overnight and calcined (500 °C in static air for 3 h, heating rate of 10 °C min^{-1}). The molar ratio of Sn to Nb could be altered by controlling the amounts of the metal salts in the solution. The resulting materials were designated SnO_2/Nb_2O_5-*x*, where *x* refers to the molar ratio of Sn to Nb. The catalysts with commercial Nb_2O_5 were prepared by an incipient wetness impregnation method.

Structural information about the Nb_2O_5 samples was obtained by powder X-ray diffraction (PXRD) (D8 FOCUS, Bruker), X-ray photoelectron spectroscopy (XPS) (ESCALAB-250, Thermo Fisher Scientific), transmission electron microscopy (TEM) (JEM-3010, JEOL), Raman spectroscopy (inVia Reflex, Renishaw, Co., UK) and UV and visible light diffuse reflection spectroscopy (UV-vis DRS, Shimadzu UV-3600). The XPS binding energies were referenced to the internal standard C 1s peak (284.5 eV). The Brunauer–Emmett–Teller (BET) method was used to calculate the specific surface area (SORPTOMATIC 1990, Thermo Electron Co.). The molar ratio of metal to Nb was determined by ICP-AES analysis. The total acid sites were determined by ammonia temperature-programmed desorption (NH_3-TPD) (OmniStar, MS200) with a thermal conductivity detector. Typically, a sample of approximately 100 mg was initially degassed at 300 °C for 2 h under a constant N_2 flow of 40 ml min^{-1}. The sample was cooled, and NH_3 was adsorbed at 90 °C for 30 min to reach saturation. Then, the ammonia supply line was shut off, and N_2 was purged at 15 ml min^{-1} for 2 h to remove physically adsorbed NH_3. The sample was then heated linearly from 90 °C to 800 °C at a rate of 10 °C min^{-1}.

The Lewis and Brønsted acid sites were investigated by FTIR using pyridine as the probe molecule. The catalyst powder was pressed into self-supporting wafers (15–20 mg) and activated in an IR cell under vacuum at 500 °C for 1 h before the adsorption experiments. The adsorption of pyridine was performed at room temperature for 1 h (excess pyridine was further evacuated for 1 h), and then a time-controlled evacuation procedure was performed at different temperatures. The FTIR spectra were measured on a Bruker Vertex 70 FTIR spectrometer with an MCT/A detector. To investigate the effect of water on the surface acidity, the samples were exposed to saturated water vapor at room temperature for 1 h and then evacuated for 30 min to remove weakly adsorbed water. Pyridine was subsequently introduced to the hydrated samples as the basic probe molecule.

The general reaction procedure was similar to a previously reported method.[28] The conversions of the triose sugars and the yields of the products were determined on a carbon basis.[29] The experiments were replicated at least three times, and the mean values were reported. The error was below 5%.

Conflicts of interest

There are no conflicts to declare.

Acknowledgements

This project was supported by Beijing Natural Science Foundation (2184101), Beijing Education Committee Science and Technology Project (KM201810017001), and the National Natural Science Foundation of China (21476021).

Notes and references

1 (*a*) A. Corma, S. Iborra and A. Velty, *Chem. Rev.*, 2007, **107**, 2411–2502; (*b*) M. S. Holm, S. Saravanamurugan and E. Taarning, *Science*, 2010, **328**, 602–605.
2 Z. Jiang, Z. Zhang, J. Song, Q. Meng, H. Zhou, Z. He and B. Han, *ACS Sustainable Chem. Eng.*, 2016, **4**, 305–311.
3 C. Chatterjee, F. Pong and A. Sen, *Green Chem.*, 2015, **17**, 40–71.
4 P. J. Deuss, K. Barta and J. G. de Vries, *Catal. Sci. Technol.*, 2014, **4**, 1174–1196.
5 D. Esposito and M. Antonietti, *Chem. Soc. Rev.*, 2015, **44**, 5821–5835.
6 (*a*) J. A. Geboers, S. Van de Vyver, R. Ooms, B. Op de Beeck, P. A. Jacobs and B. F. Sels, *Catal. Sci. Technol.*, 2011, **1**, 714–726; (*b*) P. A. Jacobs, M. Dusselier and B. F. Sels, *Angew. Chem., Int. Ed.*, 2014, **53**, 8621–8626.
7 Q. Guo, F. Fan, E. A. Pidko, W. N. van der Graaff, Z. Feng, C. Li and E. J. Hensen, *ChemSusChem*, 2013, **6**, 1352–1356.
8 K. Nakajima, J. Hirata, M. Kim, N. K. Gupta, T. Murayama, A. Yoshida, N. Hiyoshi, A. Fukuoka and W. Ueda, *ACS Catal.*, 2018, **8**, 283–290.
9 H. G. Bernal, A. M. R. Galletti, G. Garbarino, G. Busca and E. Finocchio, *Appl. Catal., A*, 2015, **502**, 388–398.
10 S. Sumiya, Y. Oumi, M. Sadakane and T. Sano, *Appl. Catal., A*, 2009, **365**, 261–267.
11 C. Yue, G. Li, E. A. Pidko, J. J. Wiesfeld, M. Rigutto and E. J. M. Hensen, *ChemSusChem*, 2016, **9**, 2421–2429.
12 G. Yang, E. A. Pidko and E. J. M. Hensen, *ChemSusChem*, 2013, **6**, 1688–1696.
13 S. Li, T. Josephson, D. G. Vlachos and S. Caratzoulas, *J. Catal.*, 2017, **355**, 11–16.

14 E. Taarning, S. Saravanamurugan, M. S. Holm, J. M. Xiong, R. M. West and C. H. Christensen, *ChemSusChem*, 2009, **2**, 625–627.
15 R. M. West, M. S. Holm, S. Saravanamurugan, J. Xiong, Z. Beversdorf, E. Taarning and C. H. Christensen, *J. Catal.*, 2010, **269**, 122–130.
16 F. de Clippel, M. Dusselier, R. Van Rompaey, P. Vanelderen, J. Dijkmans, E. Makshina, L. Giebeler, S. Oswald, G. V. Baron, J. F. M. Denayer, P. P. Pescarmona, P. A. Jacobs and B. F. Sels, *J. Am. Chem. Soc.*, 2012, **134**, 10089–10101.
17 P. Y. Dapsens, C. Mondelli and J. Perez-Ramirez, *ChemSusChem*, 2013, **6**, 831–839.
18 M. Morales, P. Y. Dapsens, I. Giovinazzo, J. Witte, C. Mondelli, S. Papadokonstantakis, K. Hungerbuhler and J. Perez-Ramirez, *Energy Environ. Sci.*, 2015, **8**, 558–567.
19 G. M. Lari, P. Y. Dapsens, D. Scholz, S. Mitchell, C. Mondelli and J. Perez-Ramirez, *Green Chem.*, 2016, **18**, 1249–1260.
20 H. T. Kreissl, K. Nakagawa, Y. Peng, Y. Koito, J. Zheng and S. C. E. Tsang, *J. Catal.*, 2016, **338**, 329–339.
21 D. M. Alonso, S. G. Wettstein and J. A. Dumesic, *Chem. Soc. Rev.*, 2012, **41**, 8075–8098.
22 K. Nemoto, Y. Hirano, K. I. Hirata, T. Takahashi, H. Tsuneki, K. I. Tominaga and K. Sato, *Appl. Catal., B*, 2016, **183**, 8–17.
23 W. Deng, P. Wang, B. Wang, Y. Wang, L. Yan, Y. Li, Q. Zhang, Z. Cao and Y. Wang, *Green Chem.*, 2018, **20**, 735–744.
24 (*a*) X. M. Yang, L. Wu, Z. Wang, J. J. Bian, T. L. Lu, L. P. Zhou, C. Chen and J. Xu, *Catal. Sci. Technol.*, 2016, **6**, 1757–1763; (*b*) J. Wang, Y. Masui and M. Onaka, *Appl. Catal., B*, 2011, **107**, 135–139; (*c*) R. Gounder, *Catal. Sci. Technol.*, 2014, **4**, 2877–2886.
25 D. Stosic, S. Bennici, V. PavloviÄ, V. Rakic and A. Auroux, *Mater. Chem. Phys.*, 2014, **146**, 337–345.
26 D. Stošić, S. Bennici, V. Rakić and A. Auroux, *Catal. Today*, 2012, **192**, 160–168.
27 L. Soh and M. J. Eckelman, *ACS Sustainable Chem. Eng.*, 2016, **4**, 5821–5837.
28 X. Wang, Y. Song, C. Huang and B. Wang, *Sustainable Energy Fuels*, 2018, **2**, 1530–1541.
29 Y. Wang, F. M. Jin, M. Sasaki, Wahyudiono, F. Wang, Z. Jing and M. Goto, *AIChE J.*, 2013, **59**, 2096–2104.
30 J. Li and H. C. Zeng, *J. Am. Chem. Soc.*, 2007, **129**, 15839–15847.
31 I. Manassidis, J. Goniakowski, L. N. Kantorovich and M. J. Gillan, *Surf. Sci.*, 1995, **339**, 258–271.
32 K. Nakajima, Y. Baba, R. Noma, M. Kitano, J. N. Kondo, S. Hayashi and M. Hara, *J. Am. Chem. Soc.*, 2011, **133**, 4224–4227.
33 A. Yu and R. Frech, *J. Power Sources*, 2002, **104**, 97–100.
34 K. Vijayarangamuthu and S. Rath, *J. Alloys Compd.*, 2014, **610**, 706–712.
35 H. Zhu, Z. Zheng, X. Gao, Y. Huang, Z. Yan, J. Zou, H. Yin, Q. Zou, S. H. Kable, J. Zhao, Y. Xi, W. N. Martens and R. L. Frost, *J. Am. Chem. Soc.*, 2006, **128**, 2373–2384.
36 J. Dijkmans, J. Demol, K. Houthoofd, S. Huang, Y. Pontikes and B. Sels, *J. Catal.*, 2015, **330**, 545–557.
37 F. Chambon, F. Rataboul, C. Pinel, A. Cabiac, E. Guillon and N. Essayem, *Appl. Catal., B*, 2011, **105**, 171–181.
38 C. B. Rasrendra, B. A. Fachri, I. G. B. N. Makertihartha, S. Adisasmito and H. J. Heeres, *ChemSusChem*, 2011, **4**, 768–777.
39 X. Wang, F. Liang, C. Huang, Y. Li and B. Chen, *Catal. Sci. Technol.*, 2016, **6**, 6551–6560.
40 X. Wang, F. Liang, C. Huang, Y. Li and B. Chen, *Catal. Sci. Technol.*, 2015, **5**, 4410–4421.
41 L. R. Merte, G. Peng, R. Bechstein, F. Rieboldt, C. A. Farberow, L. C. Grabow, W. Kudernatsch, S. Wendt, E. Lægsgaard, M. Mavrikakis and F. Besenbacher, *Science*, 2012, **336**, 889–893.